Dalton Transactions

Structural, magnetic and theoretical analyses of anionic and cationic phthalocyaninato-terbium(III) double-decker complexes: Magnetic relaxation via higher ligand-field sublevels enhanced by oxidation

Journal:	*Dalton Transactions*
Manuscript ID	DT-ART-03-2021-000775.R2
Article Type:	Paper
Date Submitted by the Author:	24-May-2021
Complete List of Authors:	Horii, Yoji; Nara Women's University, Chemistry Damjanovic, Marko; Independent Researcher Katoh, Keiichi; Josai University, Chemistry Yamashita, Masahiro; Tohoku University, Chemistry

ARTICLE

Structural, magnetic and theoretical analyses of anionic and cationic phthalocyaninato-terbium(III) double-decker complexes: Magnetic relaxation via higher ligand-field sublevels enhanced by oxidation†

Received 00th January 20xx,
Accepted 00th January 20xx

DOI: 10.1039/x0xx00000x

Yoji Horii,[a]* Marko Damjanović,* Keiichi Katoh [b]* and Masahiro Yamashita [c,d]*

Crystal structural and magnetic analyses were performed for the anionic (**1**$^-$) and cationic (**1**$^+$) forms of phthalocyaninato-Tb^{3+} double-decker single-molecule magnets (SMMs). Both charged species showed slow magnetic relaxations and magnetic hysteresis characteristic for SMMs. **1**$^+$ showed longer magnetic relaxation times (τ) and higher activation energy for spin reversal (ΔE) than **1**$^-$ did. Ligand field (LF) splitting calculated using *ab initio* methods revealed that experimental ΔE values in **1**$^-$ and **1**$^+$ were considerably larger than the first excited LF levels but rather close to the higher excited ones, indicating the magnetic relaxation via higher excited states.

Introduction

Bis tetrapyrrole lanthanoid double-decker complexes are the multi-functional molecular materials acting as rotor units of the molecular machine,[1] molecular semi-conductors[2] and single-molecule magnets (SMMs).[3] Such versatile physical properties originate from their unique structures in which the magnetic lanthanoid centre is sandwiched by redox-responsive ligands. The co-planar arrangement of the tetrapyrrole ligands results in the formation of antibonding HOMO and bonding HOMO-1 orbitals composed of the two ligand HOMO orbitals.[1, 4] Because the bond order among the π-ligands is zero, they dissociate from each other without a lanthanoid ion. In other words, lanthanoid ions of the double-decker complexes act as an imaginary adhesive which connects the tetrapyrrole ligands. The oxidation (removal of the electron from HOMO) of the double-decker complex increases the bond order between the two tetrapyrrole ligands, decreasing their face-to-face distance (*R*). The structural characterization of the redox series of the porphyrinato-lanthanoid double-decker complexes (anionic, protonated, radical and cationic form) utilizing single-crystal X-ray structural analyses was made by Yamashita *et al*.[5] In their report, the decrease in *R* upon ligand oxidations has been observed. This structural deformation couples with the magnetic properties of the lanthanoid centre. The double-decker complexes with Tb^{3+} are excellent SMMs, showing high activation energy for spin reversal and also chemical stability.[3] Ishikawa *et al.* have reported that the cationic form of the Tb^{3+} bis phthalocyaninato double-decker complex shows a larger activation energy (5.5×10^2 cm^{-1}) for spin reversal (ΔE) than that of the anionic form (2.3×10^2 cm^{-1}).[6] This behaviour has been considered to correlate with the decrease in *R* upon oxidation. The shorter the *R* is, the shorter the ligand to metal distance is. Therefore, the ligand field (LF) around Tb^{3+} ion is expected to be enhanced by the oxidation. In contrast, recent theoretical calculations utilizing the complete-active space self-consistent field (CASSCF) method for various kinds of the Tb^{3+} bis-phthalocyaninato double-decker complexes revealed that the LF splitting (and correspondingly the ΔE values) are much less dependent on the redox states and the molecular structures.[7, 8] The experimental ΔE values derived by ac magnetic susceptibility measurements for the until now reported Tb^{3+} double-decker complexes range from 200 to 900 cm^{-1},[9-11] whereas all the calculated values (first excited LF-level) reported so far are close to 300 cm^{-1}. Therefore, in the compounds showing ΔE values larger than 300 cm^{-1}, the magnetic relaxation via higher LF-levels is expected to occur.[8] Recently, the crystal structures and the magnetic properties of the dianionic form of Tb^{3+} double-decker complexes has been reported by Konarev *et al*.[12] Although the dianionic form shows a short *R* value comparable with that of the one-electron oxidized form, no sign of SMMs has been observed in it. These results suggest that there is no simple correlation between the SMM properties and the *R* values. Not only the molecular structures but also the arrangement of the molecules in the crystal affects the SMM properties. Katoh *et al.* have reported the enhancement of the SMM properties of the Tb^{3+} double-decker complexes utilizing a linear arrangement of these complexes, in which the head-to-tail arrangement of the

[a] Department of Chemistry, Faculty of Science, Nara Women's University, Nara 630-8506, Japan
[b] Department of Chemistry, Graduate School of Science, Josai University, 1-1 Keyakidai, Sakado, Saitama 350-0295, Japan
[c] Department of Chemistry, Graduate School of Science, Tohoku University, 6-3 Aza-Aoba Aramaki, Aoba-ku, Sendai, Miyagi 980-8578, Japan
[d] School of Materials Science and Technology, Nankai University, Tianjin 300350, China

† Electronic Supplementary Information (ESI) available. See DOI: 10.1039/x0xx00000x

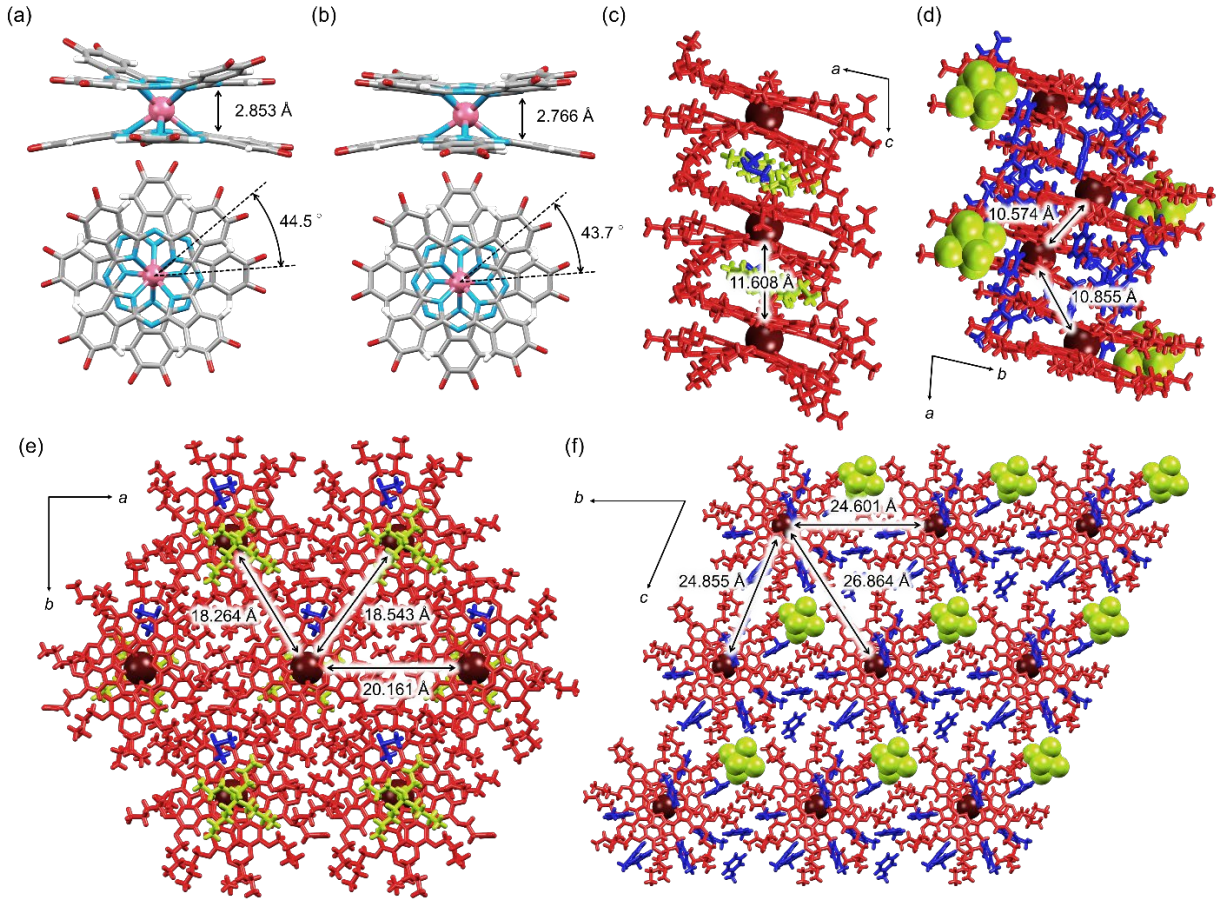

Figure 1. Crystal structures of (a) $\mathbf{1}^-$ and (b) $\mathbf{1}^+$. *n*-Butoxy chains were omitted for clarity. Pink: Tb; red: O; blue: N; grey: C. The column crystal packing of (c) $\mathbf{1}^-$ and (d) $\mathbf{1}^+$. In-plane crystal packing of (e) $\mathbf{1}^-$ and (f) $\mathbf{1}^+$. $SbCl_6^-$ units are disordered, and the conformation with highest occupancy is shown for clarity. Red, green, and blue parts represent double-decker units, counter ions and solvent molecules, respectively.

magnetic dipoles suppresses the magnetic relaxations by the quantum tunnelling of the magnetization (QTM).[9, 13] In summary, magnetic properties of the double-decker SMMs are influenced by many factors.

In this paper, we investigated the crystal structures and the magnetic properties of the anionic ($\mathbf{1}^-$) and the cationic ($\mathbf{1}^+$) forms of the Tb^{3+} double-decker complex composed of the 2,3,9,10,16,17,23,24-octabutoxy phthalocyaninato (obPc) ligands. The oxidation from $\mathbf{1}^-$ to $\mathbf{1}^+$ induces a decrease in *R*. In addition, the experimental Δ*E* value of the $\mathbf{1}^+$ is larger than that of $\mathbf{1}^-$, as reported by Ishikawa *et al*.[6] However, CASSCF calculations done in this work revealed that LF splitting is slightly decreased by the oxidation. The experimental Δ*E* values for $\mathbf{1}^-$ and $\mathbf{1}^+$ were close to the second and the third excited LF-sublevels, respectively, indicating that the Orbach process (or thermally assisted QTM) via higher sublevels is enhanced by the oxidation.

Results and discussion

X-ray structural analyses

A fine, cloudy precipitate of $\mathbf{1}^-$ has been synthesized by addition of TBA·Br to the anionic $Tb(obPc)_2^-$ species dissolved in DMSO. However, it is hard to get the single crystals suitable for X-ray analyses. Therefore, we obtained the high-quality crystals of $\mathbf{1}^-$ using the slow diffusion method. The crystal of $\mathbf{1}^-$ shows disorders on *n*-butoxy chains and DMSO molecule in the crystal packing at 263 K. However, the disorder is diminished at 120 K. Therefore, the crystal structure of $\mathbf{1}^-$ at 120 K is shown in Figure 1. The crystals of $\mathbf{1}^+$ were obtained by slow cooling of the solution of $\mathbf{1}^+$ in toluene. Crystal structures of the anionic, neutral and cationic forms of porphyrinato double-decker complexes have been reported by Yamashita *et al*.[5] They have reported that the porphyrinato-porphyrinato distances decrease upon oxidations. Similar behaviour was observed in compounds studied here. The obPc-obPc distances *R* (distance between the centroids of the coordinating N atoms of obPc) are 2.853 Å for $\mathbf{1}^-$ and 2.766 Å for $\mathbf{1}^+$ (see Figures 1a and 1b), supporting the observation that the longitudinal compression occurs by oxidation as reported by Yamashita *et al*.[5] The *R* of charge-neutral complex **1** is an intermediate between that of $\mathbf{1}^-$ and $\mathbf{1}^+$.[14] These structural changes can be explained with simple molecular orbital theory. HOMO of $\mathbf{1}^-$ is an antibonding π-orbital which has a node between the obPc ligands. The oxidation reactions remove the electrons from the antibonding HOMO of $\mathbf{1}^-$, increasing the bond order between the obPc ligands and decreasing the distance *R*. The short *R* of **1** series

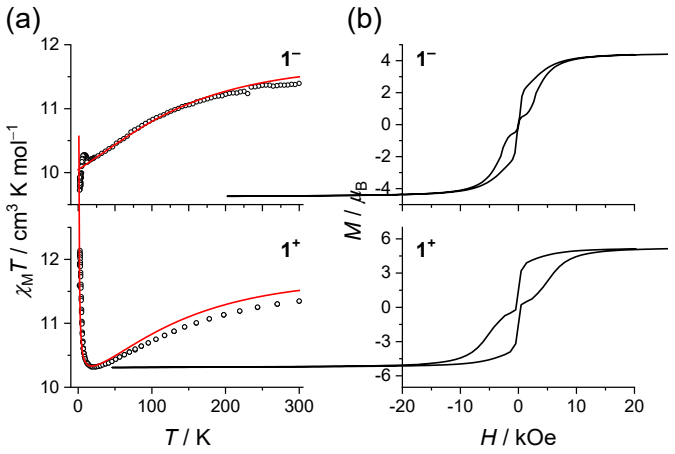

Figure 2. (a) $\chi_M T$ vs T plots for **1**⁻ and **1**⁺ at 1000 Oe dc magnetic field. Solid curves represent the theoretical $\chi_M T$ values from *ab initio* calculations. (b) Hysteresis curves for **1**⁻ and **1**⁺ at 2 K. The sweep rate of the magnetic field is 30 Oe s^{-1}.

enhances the steric hindrance between obPc ligands, causing the wide stacking angles of obPcs holding metal ions (ϑ_{obPc}~45°) at which the interligand steric hindrance is minimized.[15] The crystal packings of **1**⁻ and **1**⁺ are affected by the counter ions and the solvent molecules. **1**⁻ contains TBA^+ and DMSO as the counter cation and the crystal solvent, respectively. The flexible butyl groups of TBA^+ enable these to adopt a flat structure so that they are stacked alternatively with **1**⁻ units, thus constructing the slipped column packing along the *c*-axis (Figure 1c). The concaved distortion of the obPc ligand of **1**⁻ (see Figure 1a) may arise from the incorporated TBA^+ cation. In case of **1**⁺, the densely packed column structure composed of the double-decker units was observed (Figure 1d). Because spherical-shaped $SbCl_6^-$ ions make it difficult to construct the alternative stacking, $SbCl_6^-$ ions are located on the peripheral positions of the column packing. The shortest intermolecular Tb^{3+}-Tb^{3+} distance of **1**⁺ (10.574 Å) is shorter than that of **1**⁻ (11.608 Å) because of the densely packed column structures of **1**⁺. Inter-column Tb^{3+}-Tb^{3+} distances of **1**⁻ (18.3-20.2 Å, see Figure 1e) are shorter than those of **1**⁺ (24.6-26.9 Å, see Figure 1f), suggesting that $SbCl_6^-$ ions act as spacers to separate the columns.

Magnetic properties

The dc magnetic properties of **1**⁻ and **1**⁺ are summarized in Figure 2. The experimental and theoretical $\chi_M T$ vs *T* plots for **1** series are in agreement with each other (Figure 2a). The gradual decrease in $\chi_M T$ values in the *T* range of 300 to 20 K stems from the thermal depopulation of the LF sublevels. The hump below 15 K in **1**⁻ relates to magnetization blocking. In case of **1**⁺, an increase in $\chi_M T$ values was observed below 10 K due to intermolecular ferromagnetic interactions. $\chi_M T$ vs *T* plots for a magnetically diluted sample of cationic complex (**1**⁺*) did not show an increase in $\chi_M T$ values below 10 K (Figure S14), indicating the intermolecular ferromagnetic interactions. Theoretical $\chi_M T$ vs. *T* plots from *ab initio* calculations are consistent with the experimental data. Introduction of a mean-field parameter zJ = 0.02 cm^{-1} reproduces the increase in $\chi_M T$ values in **1**⁺, thus validating the theoretical calculations. Such ferromagnetic interactions are attributed to the intermolecular magnetic dipole-dipole interactions. Theoretical calculations indicated that magnetic easy axes of a series of **1** coincide with the C_4 axes (perpendicular to the obPc plane) as shown in Figures S15 and S16. The Tb^{3+}-Tb^{3+} distances within a column of stacked sandwich complexes are shorter than the Tb^{3+}-Tb^{3+} distances between columns in the crystal packing of **1**⁺, making the intra-column ferromagnetic interactions (head-to-tail arrangement of the magnetic dipoles) stronger than the antiferromagnetic interactions between the columns. In the *M* vs *H* plots, both complexes show butterfly-shaped magnetic hysteresis (Figure 2b). **1**⁺ shows a more open hysteresis than **1**⁻ does. The hysteresis curve of **1**⁺ at 0 Oe is open, indicating that intermolecular ferromagnetic dipole-dipole interactions on **1**⁺ act as the bias field and suppress QTM.[16]

To investigate the SMM properties of **1** series, we performed ac magnetic measurements for **1**⁻ and **1**⁺ with and without a 2000 Oe dc bias field. Both species show clear peaks in χ_M'' (imaginary part of ac magnetic susceptibilities) vs. *v* (ac frequency) plots without a bias dc magnetic field, as summarized in Figure 3a. In the presence of the bias field (2000 Oe), the χ_M'' peaks of both species show a small shift to lower *v* regions, indicating that a bias field quenches quantum tunnelling of the magnetization (QTM). Evidently, the peak tops of χ_M'' shift to the lower *v* regions by the oxidation from **1**⁻ to **1**⁺, as reported by Ishikawa *et al*.[6] All ac magnetic susceptibilities for **1** series were fitted using the generalized Debye model to acquire the spin relaxation time τ (Figures S4-S7). Arrhenius plots using the obtained τ are shown in Figure 3b. Arrhenius plots without a dc magnetic field are composed of two linear segments. The linear part in the high temperature region (above 30 K, i.e. below 0.33 K^{-1}) is attributed to an Orbach process and thermally assisted QTM (TA-QTM). The low temperature linear region (above 0,033 K^{-1}) is less temperature dependent, as indicated by a smaller slope, and is attributable to the Raman processes. Arrhenius plots at zero dc field could thus be fitted using the following equation:

$$\tau^{-1} = \tau_0{}^{-1} e^{-\Delta E/T} + CT^m \qquad (1)$$

where the first and second terms represent the Orbach (or TA-QTM) and the Raman processes, respectively.[17] Optimized parameters obtained by fitting of the experimental data are summarized in Table 1. As reported previously, the activation energy for spin reversal ΔE increased by oxidation from **1**⁻ to **1**⁺. ΔE value and frequency factor τ_0 determined by an Arrhenius fit without a bias dc field are ΔE = 449(7) cm^{-1} and τ_0= 1.3(3) × 10^{-11} s for **1**⁻ and ΔE = 551(4) cm^{-1} and τ_0 = 6.2(8) × 10^{-12} s for **1**⁺ (Figure 3b and Table 1). *m* values of the Raman process are within the range of typical lanthanoid SMMs ($2 < m < 4$). When the low *T* part of the linear region in Arrhenius plots was analysed using $\tau = \tau_0 e^{\Delta E/kBT}$, ΔE and τ_0 values were 31(1) cm^{-1} and 3.0(3) × 10^{-3} s for **1**⁻, and 48(2) cm^{-1} and 2.0(3) × 10^{-3} s for **1**⁺, respectively. Because there are no available energy levels close in magnitude to 30-50 cm^{-1}, the magnetic relaxation in the low-*T* region is attributed to the magnetic relaxation via virtual states (Raman process) rather than to Orbach (and TA-QTM) process. In the presence of bias dc field, Arrhenius plots for both complexes are linear and the contribution from the Raman

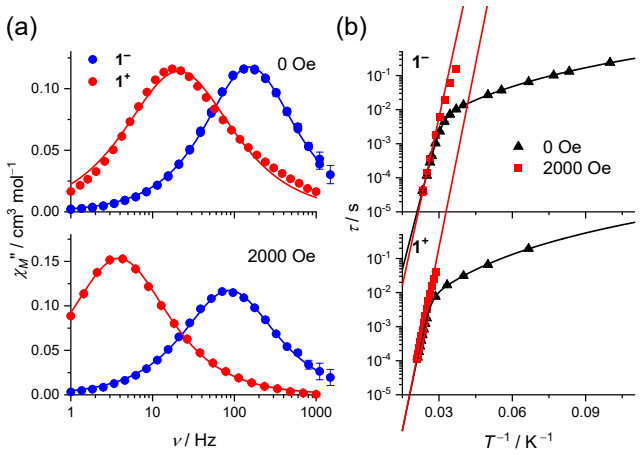

Figure 3. (a) χ_M'' vs ν plots at 35 K in the absence (0 Oe) and presence (2000 Oe) of the dc magnetic field. Solid curves represent a fit using generalized Debye model. (b) Arrhenius plots with and without a dc bias field. The black curves correspond to the simulation at 0 Oe using Eq. 1. The red lines are Arrhenius fit using the data in the T range of 35-43 K for **1**⁻ and 42-48 K for **1**⁺.

Table 1. Optimized parameters obtained by fitting the Arrhenius plots.

	τ_0 / s	ΔE / cm^{-1}	C / s^{-1} K^{-m}	m
1⁻@0 Oe	$1.3(3) \times 10^{-11}$	449(7)	$3.0(3) \times 10^{-3}$	3.15(4)
1⁻@2000 Oe	$2.2(5) \times 10^{-12}$	499(6)	-	-
1⁺@0 Oe	$6.2(8) \times 10^{-12}$	551(4)	$3.3(5) \times 10^{-4}$	3.57(5)
1⁺@2000 Oe	$3.7(3) \times 10^{-12}$	574(2)	-	-

process is negligible in the measured-T range. This is consistent with the theoretical investigation that the Raman process in the non-Kramers system is suppressed by the dc magnetic field.[18] Therefore, Arrhenius plots at 2000 Oe were fitted using Arrhenius term only. To exclude the small contribution of Raman process (tiny deviation from the linear trend at low T), the data points in the T range of 35-43 K for **1**⁻ and 42-48 K for **1**⁺ were used for Arrhenius fit. ΔE values obtained without using the Raman term are 499(6) cm^{-1} for **1**⁻ and 574(2) cm^{-1} for **1**⁺. The moderate increase in ΔE values in the presence of bias field is attributed to the suppression of TA-QTM, and QTM among the ground doublet. AC magnetic measurements were performed for magnetically diluted samples for comparison (Figures S8-S11). Arrhenius plots for magnetically diluted sample show linear trends in the measured-T range (Figures S12 and S13). The ΔE values for a magnetically diluted sample of the anionic double-decker complex (**1**⁻*) are 480(2) cm^{-1} at 0 Oe and 502(4) cm^{-1} at 2000 Oe (Table S3). Compared to undiluted **1**⁻, the diluted sample shows a tiny increase in ΔE, presumably due to the suppression of (TA-)QTM by quenching the intermolecular magnetic dipolar field. ΔE values of **1**⁺* are 528(11) cm^{-1} at 0 Oe and 530(8) cm^{-1} at 2000 Oe, and are larger than those of **1**⁻*. Therefore, the increase in ΔE values upon oxidation correlates with the modulation of electronic properties of a discrete molecule. Moreover, ΔE values of **1**⁺* are smaller than those of **1**⁺, indicating that intermolecular ferromagnetic dipole-dipole interactions in **1**⁺ block magnetic

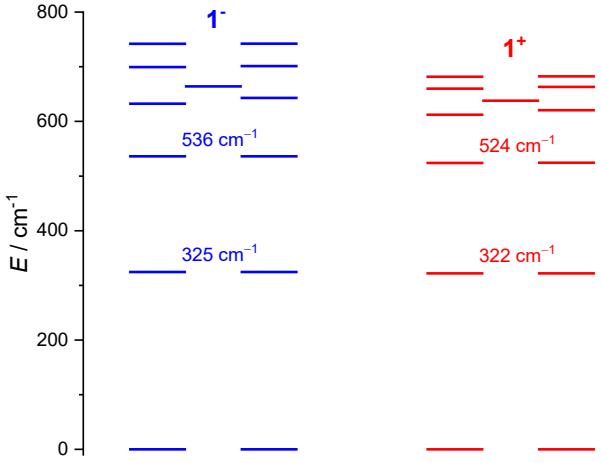

Figure 4. LF splitting from CASSCF calculations using the crystal structure coordinates of **1**⁻ and **1**⁺.

relaxations due to exchange bias effect, as reported by Katoh *et al*.[9, 19] In other words, the ferromagnetic dipole-dipole interactions act as if a dc magnetic field is applied along the magnetic easy axis (C_4 axis of the double-decker complex), suppressing (TA-)QTM.

To validate experimental ΔE values, we performed the complete-active-space self-consistent field (CASSCF) method and spin-orbit coupling calculations with MOLCAS[20] for **1**⁻ and **1**⁺. This was done by using the modified crystal coordinates, where the *n*-butoxy chains were replaced by methoxy groups. Figure 4 summarizes 13 of the LF sublevels (the energy values are summarized in Table S12). A series of **1** shows strong axial magnetic anisotropy as reported previously, where the ground quasi-doublet is composed by almost pure |±6> states.[3, 8, 21] The first and the second excited states are also quasi-doublet states composed of almost pure |±5> and |±4>, respectively. In contrast, the electronic states of energy levels higher than the second excited sublevel (above 600 cm^{-1}) mix with each other, inducing a large (1-10 cm^{-1}) tunnelling gap. The energy gap between the ground doublet and the first excited doublet often corresponds to the experimental ΔE values. Recent SMMs having high ΔE values show the Orbach process and thermally assisted QTM (TA-QTM) via higher excited sublevels.[22-26] The experimental ΔE values for **1**⁻ (499(6) cm^{-1} at 2000 Oe) and **1**⁺ (574(2) cm^{-1} at 2000 Oe) are close to theoretical energy levels of the second (536 cm^{-1} for **1**⁻) and the third excited quasi-doublet (612-620 cm^{-1} for **1**⁺), respectively, rather than those of the first excited quasi-doublet (325 cm^{-1} for **1**⁻ and 322 cm^{-1} for **1**⁺). These results indicate the Orbach process and TA-QTM via higher LF-levels. It is known that the coincidence of the magnetic easy axes of ground and excited doublets decrease the magnetic transition probabilities and enhance the magnetic relaxation via higher sublevels.[27] According to the *ab initio* calculations, the second exited states in studied series of **1** are composed of almost pure |±4> terms, hence the linearity of magnetic easy axis between the ground, first and second exited states is sustained (Tables S13 and S14). Although *ab initio* calculations indicate that LF splitting of **1**⁻ and **1**⁺ are similar with

each other, the experimental Δ*E* value of $\mathbf{1}^{+}$ is larger than that of $\mathbf{1}^{-}$. In **1** series, a small portion of |±3> and |±2> mixes to the first excited and second excited doublet (|±5> and |±4>), respectively. The amount of such mixing in $\mathbf{1}^{+}$ is smaller than that in $\mathbf{1}^{-}$. The mixing of wavefunctions relates to the calculated *g*-tensors for $\mathbf{1}^{-}$ and $\mathbf{1}^{+}$ (Table S15). *z*-component of the *g*-tensor (g_z) for third excited quasi-doublet of $\mathbf{1}^{+}$ (g_z = 8.13) is substantially larger than that of $\mathbf{1}^{-}$ (g_z = 7.74), indicating the stronger axial magnetic anisotropy of the excited states of $\mathbf{1}^{+}$. These improved axial magnetic anisotropies of $\mathbf{1}^{+}$ enhance the relaxation via higher excited states due to suppression of the TA-QTM. As reported by Layfield *et al.*, the SMM properties also depend on the molecular vibration modes.[28] Suppression of the vibrational modes which couple with the LF levels prohibit the magnetic relaxations.[19] Though significant changes in the vibrational frequencies upon oxidations were not seen in the frequency calculations (Figure S3 and Table S2), slight modulation of the vibrations cannot be ruled out from the possible mechanism for the enlargement of the Δ*E* value. In addition, intermolecular magnetic interactions should affect the SMM behaviour. Katoh *et al*. have reported that the ferromagnetic arrangement of the magnetic dipoles of the Tb^{3+} ions enhances the SMM properties of the double-decker complexes.[9, 29] As proved by the dc magnetic measurements, intermolecular ferromagnetic interactions enhanced in the 1D crystal packing of $\mathbf{1}^{+}$ act as the exchange bias.[16] In addition, Δ*E* values of oxidized double-decker complexes decrease upon magnetic dilution. These results indicate that intermolecular ferromagnetic dipole-dipole interactions to some extent block magnetic relaxations via second excited levels, enhancing TA-QTM via third excited sub-levels.

Experimental Section

The neutral form of the *n*-butoxy substituted double-decker complex (**1**) and phenoxathiin hexachloroantimonate ($SbCl_6$·Ox) were synthesized according to the literature methods.[30] Tetrabutylammonium bromide (TBA·Br), hydrazine monohydrate and all the solvents used in the reaction were purchased from FUJIFILM Wako Pure Chemical Corporation.

Synthesis of $\mathbf{1}^{-}$

The synthesis of bulk amount of $\mathbf{1}^{-}$ has been reported by our group.[31] Single crystals suitable for SXRD measurements were prepared using the solvent diffusion method shown below. To a 2 mL microtube, 10 mg of **1** (0.0043 mmol), 100 μL of chloroform, 100 μL of dimethyl sulfoxide, 20 μL of hydrazine monohydrate (0.41 mmol) were added and mixed using ultrasonication until the color of the solution turned blue. Slow diffusion of dimethyl sulfoxide containing ~80 mM of tetrabutylammonium bromide for 2 weeks gave red block crystals of $\mathbf{1}^{-}$ suitable for SCXRD measurements (7.6 mg, 67%). Elemental analysis calculated (%) for $C_{144}H_{196}N_{17}O_{16}Tb$: C 67.03, H 7.66, N 9.23; found: C 66.80, H 7.49, N 9.17.

Synthesis of $\mathbf{1}^{+}$

To a 10 mL vial, 25 mg of **1** (0.011 mmol), 8.2 mg of $SbCl_6$·Ox (0.015 mmol) and 3 mL of toluene were added and mixed using ultrasonication. The vial was put in the oven and heated at 100 °C for 5 h, followed by slow cooling down to room temperature over 12 h afforded the crystalline $\mathbf{1}^{+}$ (22 mg, 66%). Elemental analysis calculated (%) for $C_{128}H_{160}N_{16}O_{16}TbSbCl_6$: C 57.53, H 6.04, N 8.39; found: C 57.26, H 5.92, N 8.23.

Conclusions

We presented the detailed structural and magnetic analyses for anionic and cationic Tb^{3+} phthalocyaninato double-decker complexes. Crystal structures and crystal packings of the double-decker units depend on the charges of the molecules and the shape of the counter ions. $\mathbf{1}^{+}$ shows large magnetic hysteresis and slower magnetic relaxation times than $\mathbf{1}^{-}$ does because of the intermolecular ferromagnetic interactions enhanced in the crystal packing of $\mathbf{1}^{+}$. The strong axial magnetic anisotropy of **1** series was validated by *ab initio* calculations. Experimental Δ*E* values for **1** series are larger than the first excited sub-levels, indicating the magnetic relaxations via higher sub-levels. Our results suggest that the experimental Δ*E* values which vary from 200 to 900 cm^{-1} for all the Tb^{3+} double-decker complexes reported so far stem from the differences in the excited LF sublevels participating in the Orbach process and TA-QTM. In contrast to the previous assumptions, no significant enhancement of the LF splitting via ligand oxidations were predicted from *ab initio* calculations upon oxidation of $\mathbf{1}^{-}$. However, the excited quasi-doublets of $\mathbf{1}^{+}$ are better protected from the contamination by small $|m_J>$ states. Better axiality of the excited states in $\mathbf{1}^{+}$ is likely to enhance the magnetic relaxation via the third excited quasi-doublet. In addition, intermolecular ferromagnetic interactions induced by the 1D packing of the $\mathbf{1}^{+}$ units act as the exchange bias, enhancing the SMM properties.

Author Contributions

All authors contribute equally.

Conflicts of interest

There are no conflicts to declare.

Acknowledgements

This work was financially supported by JSPS KAKENHI Grant Numbers JP14J02656 (Y.H.), JP24750119 (K.K.), JP15K05467 (K.K.), JP20225003 (M.Y.), JP18K14242 (Y.H.), JP19H05631 (M.Y.) and JST, CREST Grant Number JPMJCR12L3 (M.Y.), Japan. M.Y. thanks the 111 project (B18030) from China for the support. We thank Prof. Dr. Takashi Kajiwara (Nara Women's University) for magnetic measurements and powder X-ray diffraction measurements.

Notes and references

1. K. Tashiro, K. Konishi and T. Aida, *J. Am. Chem. Soc.*, 2000, **122**, 7921-7926.
2. P. Turek, P. Petit, J. J. Andre, J. Simon, R. Even, B. Boudjema, G. Guillaud and M. Maitrot, *J. Am. Chem. Soc.*, 1987, **109**, 5119-5122.
3. N. Ishikawa, M. Sugita, T. Ishikawa, S.-y. Koshihara and Y. Kaizu, *J. Am. Chem. Soc.*, 2003, **125**, 8694-8695.
4. S. Takamatsu and N. Ishikawa, *Polyhedron*, 2007, **26**, 1859-1862.
5. K.-i. Yamashita, T. Yamanaka, N. Sakata and T. Ogawa, *Chem. Asian J.*, 2018, **13**, 1692-1698.
6. S. Takamatsu, T. Ishikawa, S.-y. Koshihara and N. Ishikawa, *Inorg. Chem.*, 2007, **46**, 7250-7252.
7. L. Ungur and L. F. Chibotaru, *Chem. Eur. J.*, 2017, **23**, 3708-3718.
8. R. Pederson, A. L. Wysocki, N. Mayhall and K. Park, *J. Phys. Chem. A*, 2019, **123**, 6996-7006.
9. K. Katoh, S. Yamashita, N. Yasuda, Y. Kitagawa, B. K. Breedlove, Y. Nakazawa and M. Yamashita, *Angew. Chem. Int. Ed.*, 2018, **57**, 9262-9267.
10. L. Malavolti, M. Mannini, P.-E. Car, G. Campo, F. Pineider and R. Sessoli, *J. Mater. Chem. C*, 2013, **1**, 2935-2942.
11. K. Wang, F. Ma, D. Qi, X. Chen, Y. Chen, Y.-C. Chen, H.-L. Sun, M.-L. Tong and J. Jiang, *Inorg. Chem. Front.*, 2018, **5**, 939-943.
12. D. V. Konarev, S. S. Khasanov, M. S. Batov, A. G. Martynov, I. V. Nefedova, Y. G. Gorbunova, A. Otsuka, H. Yamochi, H. Kitagawa and R. N. Lyubovskaya, *Inorg. Chem.*, 2019, **58**, 5058-5068.
13. M. Yamashita, *Bull. Chem. Soc. Jpn.*, 2021, **94**, 209-264.
14. K. Katoh, H. Isshiki, T. Komeda and M. Yamashita, *Coord. Chem. Rev.*, 2011, **255**, 2124-2148.
15. N. Koike, H. Uekusa, Y. Ohashi, C. Harnoode, F. Kitamura, T. Ohsaka and K. Tokuda, *Inorg. Chem.*, 1996, **35**, 5798-5804.
16. W. Wernsdorfer, N. Aliaga-Alcalde, D. N. Hendrickson and G. Christou, *Nature*, 2002, **416**, 406-409.
17. A. Abragam and B. Bleaney, *Electron paramagnetic resonance of transition ions*, OUP Oxford, 2012.
18. L. T. A. Ho and L. F. Chibotaru, *Phys. Rev. B*, 2018, **97**, 024427.
19. T. Yamabayashi, M. Atzori, L. Tesi, G. Cosquer, F. Santanni, M.-E. Boulon, E. Morra, S. Benci, R. Torre, M. Chiesa, L. Sorace, R. Sessoli and M. Yamashita, *J. Am. Chem. Soc.*, 2018, **140**, 12090-12101.
20. F. Aquilante, J. Autschbach, R. K. Carlson, L. F. Chibotaru, M. G. Delcey, L. De Vico, I. Fdez. Galván, N. Ferré, L. M. Frutos, L. Gagliardi, M. Garavelli, A. Giussani, C. E. Hoyer, G. Li Manni, H. Lischka, D. Ma, P. Å. Malmqvist, T. Müller, A. Nenov, M. Olivucci, T. B. Pedersen, D. Peng, F. Plasser, B. Pritchard, M. Reiher, I. Rivalta, I. Schapiro, J. Segarra-Martí, M. Stenrup, D. G. Truhlar, L. Ungur, A. Valentini, S. Vancoillie, V. Veryazov, V. P. Vysotskiy, O. Weingart, F. Zapata and R. Lindh, *J. Comput. Chem.*, 2016, **37**, 506-541.
21. N. Ishikawa, M. Sugita, T. Okubo, N. Tanaka, T. Iino and Y. Kaizu, *Inorg. Chem.*, 2003, **42**, 2440-2446.
22. R. J. Blagg, L. Ungur, F. Tuna, J. Speak, P. Comar, D. Collison, W. Wernsdorfer, E. J. McInnes, L. F. Chibotaru and R. E. Winpenny, *Nat. Chem.*, 2013, **5**, 673-678.
23. Y.-S. Ding, N. F. Chilton, R. E. P. Winpenny and Y.-Z. Zheng, *Angew. Chem. Int. Ed.*, 2016, **55**, 16071-16074.
24. C. A. P. Goodwin, F. Ortu, D. Reta, N. F. Chilton and D. P. Mills, *Nature*, 2017, **548**, 439-442.
25. F.-S. Guo, B. M. Day, Y.-C. Chen, M.-L. Tong, A. Mansikkamäki and R. A. Layfield, *Angew. Chem. Int. Ed.*, 2017, **56**, 11445-11449.
26. D. Aravena, *J. Phys. Chem. Lett.*, 2018, **9**, 5327-5333.
27. L. Ungur and L. F. Chibotaru, *Phys. Chem. Chem. Phys.*, 2011, **13**, 20086-20090.
28. F.-S. Guo, B. M. Day, Y.-C. Chen, M.-L. Tong, A. Mansikkamäki and R. A. Layfield, *Science*, 2018, **362**, 1400-1403.
29. T. Yamabayashi, K. Katoh, B. K. Breedlove and M. Yamashita, *Molecules*, 2017, **22**.
30. Y. Horii, M. Damjanovic, M. R. Ajayakumar, K. Katoh, Y. Kitagawa, L. Chibotaru, L. Ungur, M. Mas-Torrent, W. Wernsdorfer, B. K. Breedlove, M. Enders, J. Veciana and M. Yamashita, *Chem. Eur. J.*, 2020, **26**, 8621-8630.
31. M. Damjanović, T. Morita, K. Katoh, M. Yamashita and M. Enders, *Chem. Eur. J.*, 2015, **21**, 14421-14432.